RESEARCH/REVIEW ARTICLE

Influence of winter sea-ice motion on summer ice cover in the Arctic

Noriaki Kimura,[1] Akira Nishimura,[2] Yohei Tanaka[1] & Hajime Yamaguchi[1]

[1] Graduate School of Frontier Sciences, University of Tokyo, 5-1-5 Kashiwanoha Kashiwa 277-8561, Japan
[2] School of Engineering, University of Tokyo, 5-1-5 Kashiwanoha Kashiwa 277-8561, Japan

Keywords
Sea ice; Arctic; satellite remote-sensing; interannual variability; AMSR-E data.

Correspondence
Noriaki Kimura, Kiban-Tou 6H1, 5-1-5 Kashiwanoha Kashiwa 277-8561, Japan.
E-mail: kimura@1.k.u-tokyo.ac.jp

Abstract

Summer sea-ice cover in the Arctic varies largely from year to year owing to several factors. This study examines one such factor, the relationship between interannual difference in winter ice motion and ice area in the following summer. A daily-ice velocity product on a 37.5-km resolution grid is prepared using the satellite passive microwave sensor Advanced Microwave Scanning Radiometer—Earth Observing System data for the nine years of 2003–2011. Derived daily-ice motion reveals the dynamic modification of the winter ice cover. The winter ice divergence/convergence is strongly related to the summer ice cover in some regions; the correlation coefficient between the winter ice convergence and summer ice area ranges between 0.5 and 0.9 in areas with high interannual variability. This relation implies that the winter ice redistribution controls the spring ice thickness and the summer ice cover.

With recent attention on the decrease of the Arctic ice area in the context of global warming, a greater understanding of sea-ice processes is required. The Arctic ice extent in September has diminished with a trend of −10.1% per decade between 1996 and 2007 (Comiso et al. 2008). This trend is caused by several factors, such as atmospheric conditions (Rigor et al. 2002; Perovich et al. 2007) and ocean conditions (Shimada et al. 2006). The thickness of the Arctic sea ice has also decreased recently. Kwok et al. (2009) reported that winter Arctic ice volume decreased by 21% during 2003–08.

Interannual variability with shorter timescales is also noticeable in the Arctic ice cover. Figure 1 shows the ice edges on 10 September in the nine years from 2003 to 2011. Ice cover here is defined by ice concentration of more than 15%. Wide interannual variability in the ice cover is noticeable around the East Siberian Sea; this is mainly due to the exceptional reduction in 2007. The yearly difference in summer ice cover can be explained partly by the interannual change in wind forcing (e.g., Ogi et al. 2010).

The Arctic Ocean is nearly fully covered by sea ice until April or May, after which time interannual differences in ice area become noticeable. It is clear that weather conditions during the melt season are major determinants of the summer ice cover. Another possible cause of the interannual difference in the summer ice cover is preconditioning for melting, in other words, ice thickness in spring before the start of melting.

Thickness of sea ice has been observed by field experiments (e.g. Melling & Riedel 1995), submarine (e.g., Rothrock et al. 2008) and satellite sensors such as CryoSat and ICESat (e.g., Kwok et al. 2009). However, at the moment these observations are insufficient in their spatial and temporal coverage, observation period or their accuracy to resolve the interannual difference of ice thickness in spring.

To reveal the spring ice properties and examine the processes behind the interannual difference in summer ice cover, this study focuses on the winter ice motion. Large interannual variability seen in the winter ice motion and resulting redistribution of the ice should affect the ice properties such as thickness distribution in spring. This study aims to examine the relationship between interannual differences in winter ice motion and ice area in the following summer. If the relation is significant, we can potentially improve predictions of the summer ice cover by the end of spring.

Citation: *Polar Research* 2013, *32*, 20193, http://dx.doi.org/10.3402/polar.v32i0.20193

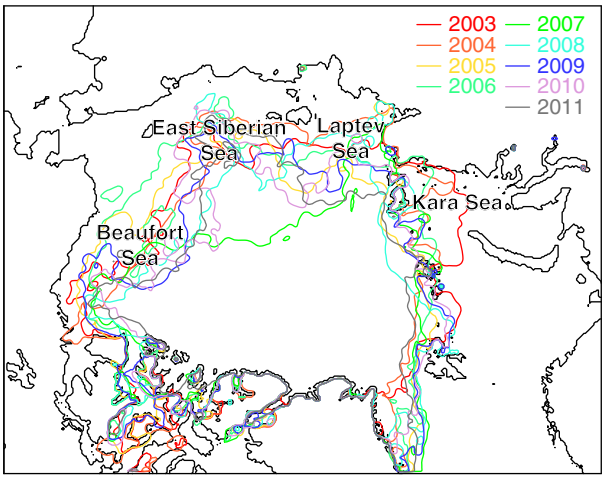

Fig. 1 The ice edge on 10 September for the nine years of 2003–2011.

Data

We have prepared a daily-ice velocity data set for winter season between 1 December and 30 April, which is the same one used in our study on the Southern Ocean (Kimura & Wakatsuchi 2011), calculated from images of the Microwave Scanning Radiometer—Earth Observing System (AMSR-E) satellite. Ice velocity is computed from the gridded brightness temperature of 89-GHz horizontal and vertical polarization channels (Cavalieri et al. 2004), which is binned to square pixels of 6.25 × 6.25 km by the National Snow and Ice Data Center (NSIDC). The procedure for detecting ice motion, which has been improved in our studies (e.g., Kimura & Wakatsuchi 2000, 2004), is based on the maximum cross-correlation method described by Ninnis et al. (1986) and Emery et al. (1991). This method determines the spatial offset that maximizes the cross-correlation coefficient between two brightness temperature arrays in consecutive images separated by 24 h. For this procedure, 6 × 6 grid cell (37.5 × 37.5 km) arrays are utilized. As the first step, we detect the ice motion vector on one-grid (6.25 km) interval. Next, detections of a false match are automatically filtered out by the following: (1) eliminate the vectors with less than 0.5 of the maximum cross-correlation coefficient; (2) pick up the reliable vectors with more than 0.72 of the correlation coefficient; (3) as for the results with 0.5–0.72 of the correlation coefficient, eliminate results in cases where the difference from the reliable vectors within a radius of 100 km is more than 14.4 cm/s (2 pixel/day). Filtered ice motion vector in a 6.25 × 6.25 km grid is organized into a 37.5 × 37.5 km grid data set. Each vector in this data set is made up by using the 6 × 6 of calculated vectors in the 6.25 km grid. In this procedure, more than six vectors are utilized for each resulting vector. If the number of the available vector is less than six, that grid is regarded as missing data. The discrimination of the resulting vector, which consists of 6–36 velocities, becomes higher than the detection limit of the original displacement vector of 7.2 cm/s (6.25 km [1 pixel]/1 day). After that, the daily data are calculated as a mean value of four data derived from the horizontal polarization channel image of ascending and descending data, and the vertical polarization channel image of ascending and descending data. At this stage, 86.9, 86.7, 85.5, 85.7 and 87.4% of ice vector is successfully derived for December, January, February, March and April, respectively. The remaining gap in the data was filled through spatial interpolation using the available data from the surrounding eight grids. After these processes, we construct a daily-ice velocity data set without missing data over the sea-ice area on a 37.5 × 37.5 km grid for the nine-year period 2003–2011.

To evaluate the error in the data set, we compare the derived ice velocity with buoy position data from the International Arctic Buoy Programme (IABP; Colony & Rigor 2002) distributed by NSIDC. We use position data at 1200 UT of all 58 buoys so that their duration covers the period between 1 December 2009 and 30 April 2010 or between 1 December 2010 and 30 April 2011. Figure 2a and b presents scatterplots of daily AMSR-E-derived sea-ice speed versus buoy speed for horizontal and vertical components, respectively. Ice velocity at each buoy position is calculated from neighbouring grid data at the same day weighted by Gaussian function, with 37.5 km of e-folding scale and 56.25 km of influence radius, of distance from the buoy position. The buoy velocity at any day is calculated from movement of buoy position between that day and the next day. Based on the coincident 4868 AMSR-E and buoy vectors, correlation coefficients between them are 0.930 for horizontal direction and 0.932 for vertical direction. Regression coefficients defined by the first principal component of plots are 1.027 (horizontal) and 1.045 (vertical); AMSR-E derived ice motion is 2.7 and 4.5% overestimate of the ice speed. Estimated biases are small and are not taken into account in any following analyses. The root mean square errors (RMSE) of the AMSR-E ice velocity without any correction to the buoy velocity are 1.46 cm/s (horizontal) and 1.35 cm/s (vertical). Figure 2c presents a comparison between trajectories of 30 buoys from 1 December to 30 April for 2009–2010 and 2010–11, and tracks of particles calculated from the AMSR-E derived ice velocity starting from the buoy location on 1 December and calculated independently from the buoy motion. The AMSR-E derived data set can reproduce the ice track with high accuracy on a variety of temporal scales from daily changes to

Citation: *Polar Research* 2013, *32*, 20193, http://dx.doi.org/10.3402/polar.v32i0.20193

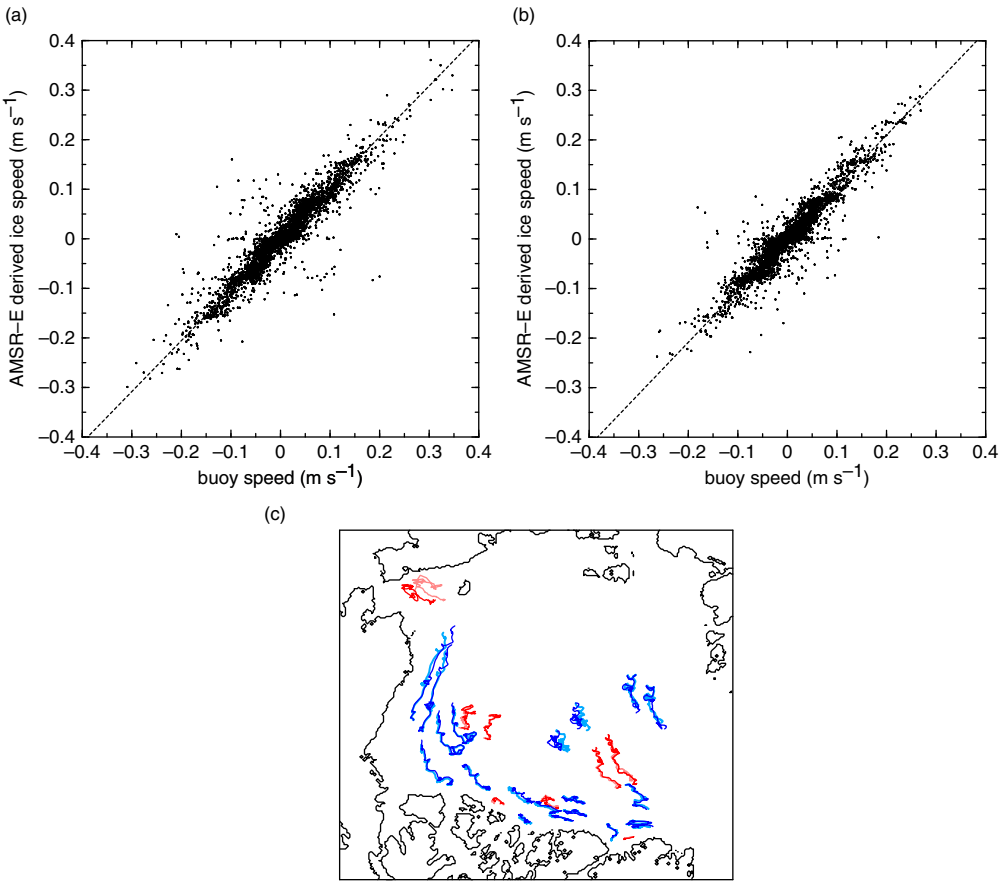

Fig. 2 Comparison of drifting buoy motion and Microwave Scanning Radiometer—Earth Observing System (AMSR-E) satellite-derived ice motion. (a) Scatterplot of ice drift speed derived from AMSR-E versus buoy speed based on 4868 daily data, for horizontal direction of (c). b) Same as (a) but for vertical direction. Dotted lines are regression lines defined by the first principal component of plots. (c) Trajectories of 30 buoys (bold lines) and those of particles calculated from the AMSR-E derived ice velocity (thin lines) during one year from 1 December to 30 April 2009–2010 (blue lines) and 2010–11 (red lines).

long-term movement. The difference in the two locations is less than 50 km after five months of travelling.

This study also uses AMSR-E-derived daily-ice concentration on a 12.5-km resolution grid (Cavalieri et al. 2003), based on the enhanced National Aeronautical and Space Administration Team (NT2) ice-concentration algorithm (Markus & Cavalieri 2000).

Characteristics of sea-ice motion during winter

To visualize the dynamic redistribution of sea ice, movement of particles spread over the ice-covered area is calculated. About 10 000 particles are arranged at an interval of 37.5 km over the ice area on 1 December of each year. Initial position of the particles is changed year to year according to the interannual difference in the ice area. Daily displacement of particles released on the day is calculated from the AMSR-E-derived ice velocity on one-day time steps. Ice velocity at each particle position is derived from neighbouring grids weighted by Gaussian function of distance between the particle position and data grid as the same for the error evaluation in the previous section.

Since sea-ice concentration within the Arctic is near 100% during winter, ice divergence and convergence yield new ice production and dynamic thickening, respectively. Figure 3a–d and 3e–h presents the temporal change of the particle distribution in winter from 1 December to 30 April for 2004–05 and 2007–08. The spatial inhomogeneity of the particle distribution becomes significant with time. Though there are obvious interannual differences, particles generally become sparse in the Kara, Laptev and Beaufort seas in contrast to the convergence of the particles in the East Siberian Sea. This regional pattern is similar to that shown by Kwok (2006). In the convergence area, the density of the particles becomes higher

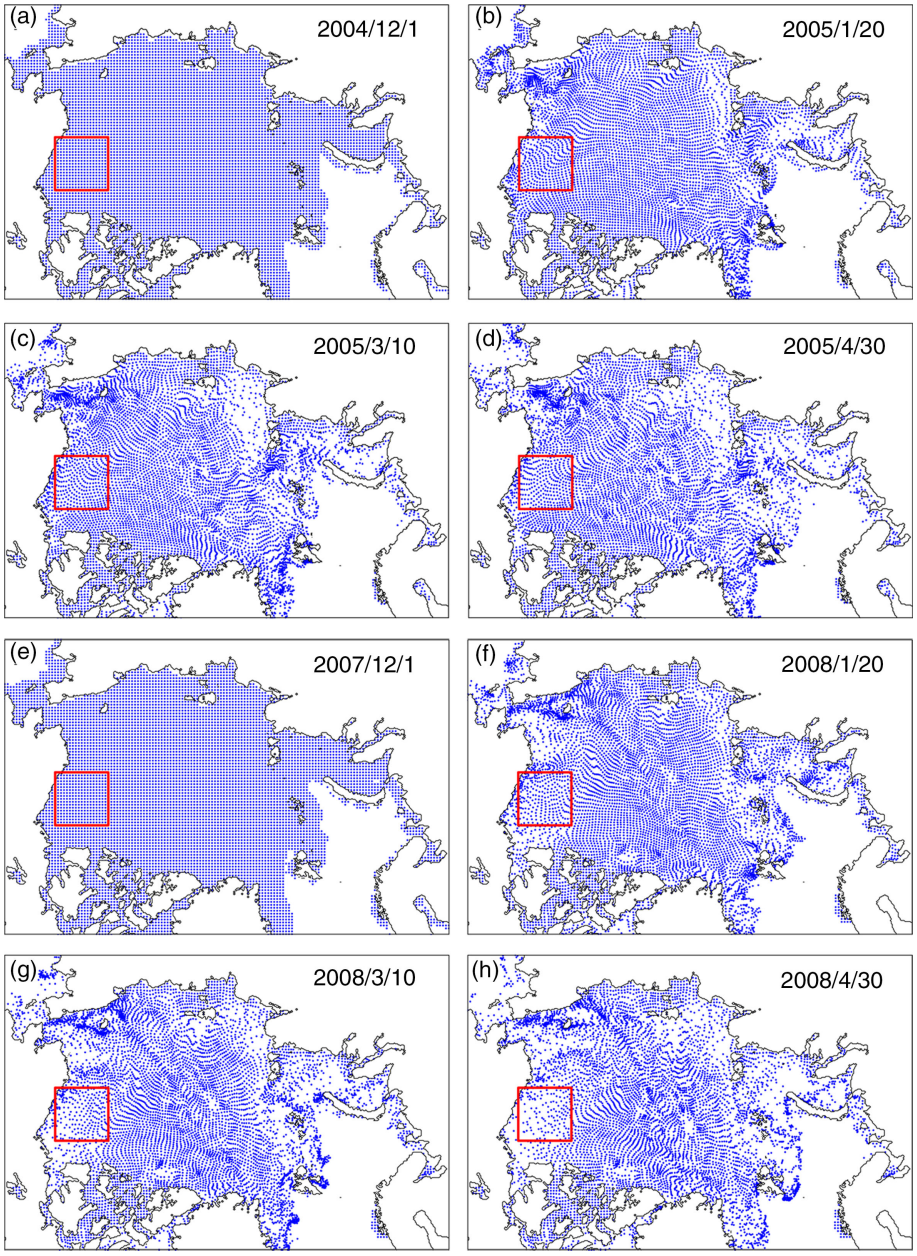

Fig. 3 Distribution of migrating particles for (a) 1 December 2004, (b) 20 January 2005, (c) 10 March 2005, (d) 30 April 2005, (e) 1 December 2007, (f) 20 January 2008, (g) 10 March 2008 and (h) 30 April 2008, which are first arrayed over the ice-covered area on 1 December and are moved based on the Microwave Scanning Radiometer—Earth Observing System satellite-derived daily-ice velocity.

than the initial distribution. This means that dynamic deformation and accompanied thickening of sea ice through rafting or ridging of ice floes is occurring. In contrast, ice divergence promotes the formation of leads and polynyas, which is associated with new ice production; it results in a higher fraction of thin ice compared with the convergence areas. As a result, ice thickness in divergence areas becomes lower compared with convergence areas. We can consider that summer ice cover has a relation to the ice motion before spring probably through the dynamic change of ice thickness.

For example, in the Beaufort Sea, sea-ice cover retreats between May and September in both 2005 and 2008 (Fig. 4). In 2008, more than 60% of the particles were exported from this region between 1 December and 30 April, that is, the ice area at the end of April consists of more than 60% thin ice produced after December. In response to the thinning, ice area in 2008 decreased

Citation: *Polar Research* 2013, *32*, 20193, http://dx.doi.org/10.3402/polar.v32i0.20193

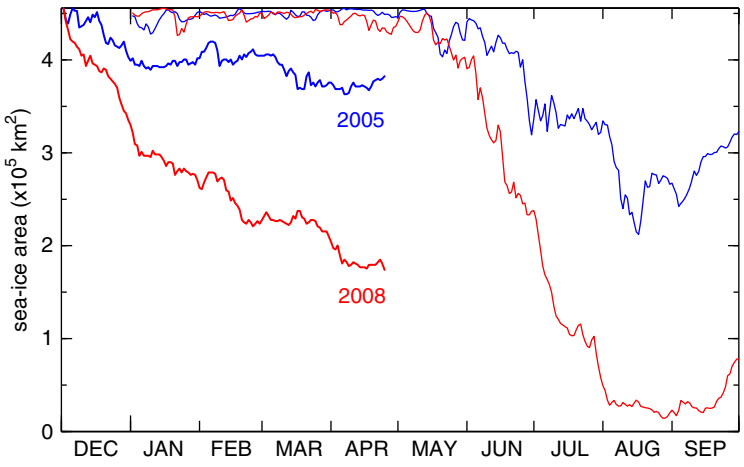

Fig. 4 Bold lines indicate the fraction of sea ice existing since before 1 December and the temporal evolution of the number of particles within that part of the Beaufort Sea bounded by the red squares shown in Fig. 3 for 2005 and 2008 The unit of the particle number is converted to ice area (km^2) by multiplying by 37.5 ×37.5, under the assumptions that each particle represents a 37.5 ×37.5 km of area with 100% ice concentration and that ice melting during December and April is negligible. Thin lines show the corresponding total sea-ice area within the same region calculated from the daily-ice concentration.

rapidly after May. In contrast, in 2005 there was little export of ice during winter and the resulting predominantly thick ice resulted in the slow decrease of total sea-ice area during the melting season. This relation between the winter ice redistribution and retreat speed of the total ice area is also seen in other areas as described in the following section.

Relationship between winter ice motion and summer ice area

This section examines the relationship between the winter ice redistribution and summer ice area based on the nine years of 2003–2011 for 108 domains defined by 375 × 375 km^2 (10 × 10 pixels, 1.4×10^5 km^2). Here, we will focus on two quantities, total ice area on 10 September (IA9 hereafter) and the number of particles converted into the area on 30 April (as seen in Fig. 3d and h) moved from 1 December (NP4 hereafter); the unit of both is square kilometres. IA9 is calculated by adding up the ice concentration within each domain. NP4 is derived by multiplying the number of particles by 37.5 × 37.5 km^2, as described in the previous section. The standard deviations of IA9 and NP4 for each domain are presented in Fig. 5. The interannual variability of IA9 is large around the marginal summer ice area. The large variability of NP4 is noticeable near the coast.

Based on nine data points of the nine years' data, Fig. 6a shows the correlation coefficient between NP4 and IA9 of same year, for each domain. There are high correlation coefficients between the winter ice redistribution and summer ice area in several domains. The relationship is

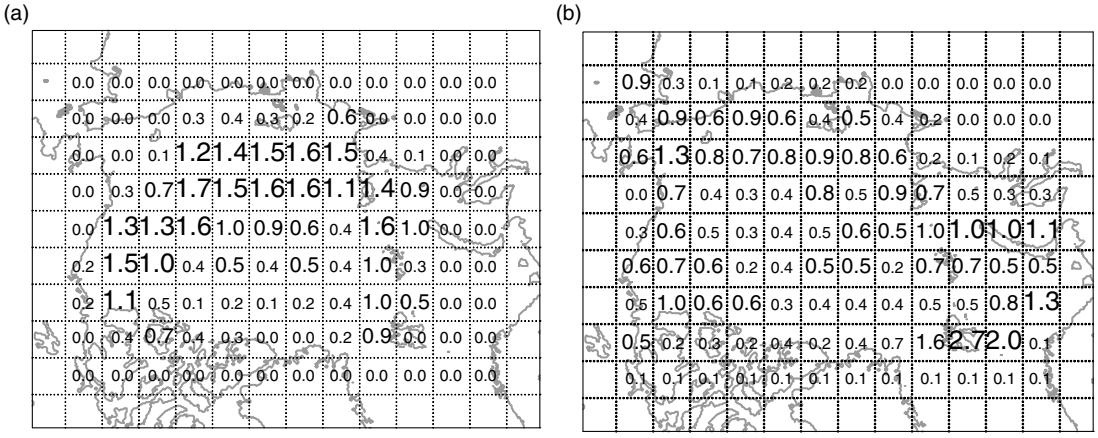

Fig. 5 Standard deviation of (a) sea-ice area on 10 September (IA9) and (b) number of particles (NP4) on 30 April for 108 domains in 10^4 km^2.

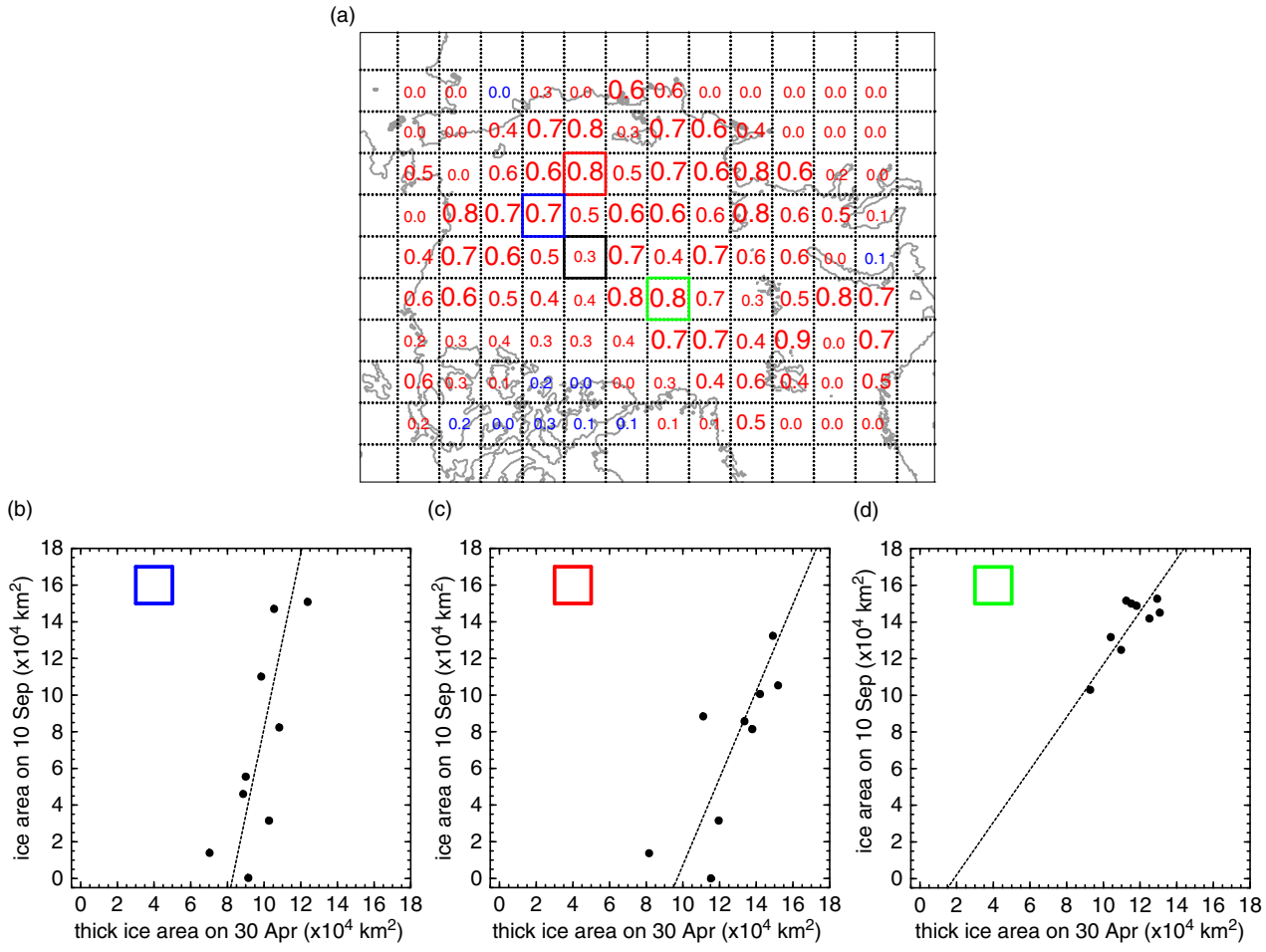

Fig. 6 (a) Correlation coefficient between the number of particles on 30 April migrated from 1 December (NP4), and the total ice area on 10 September (IA9) of the same year for 108 domains, based on the nine years' data. Panels below are scatterplots of IA9 versus NP4 for domains shown by (b) blue, (c) red and (d) green rectangles. Dotted lines in these panels show regression lines defined by the first principal component of plots.

significant in 18 domains at a 95% confidence level based on a two-sided *t*-test, that is, domains with a correlation coefficient of more than 0.67. The strong relationship in these domains supports the scenario that a greater ice divergence or outflow in winter and resulting thinner ice cover in spring contributes to the smaller ice area in summer. Figure 6b–d comprises scatterplots of IA9 versus NP4. Regression coefficients (slope of the regression lines) defined by the first principal component of plots are 4.8 (b), 2.4 (c) and 1.4 (d). These values larger than 1.0 means that interannual difference in NP4 is not directly related to that in IA9; small difference in NP4 results in the larger difference in IA9. There are some positive feedback processes or indirect mechanisms between the ice motion in winter (ice thickness in spring) and subsequent ice melting.

Figure 7 shows the scatterplot of the derived correlation coefficient (shown in Fig. 6a) versus standard deviation of IA9 (shown in Fig. 5a) for the 108 domains. Correlation is significant only in 17% of domains in all 108 domains. The percentage becomes 36% when we focus only on domains with more than 1.2×10^4 km^2 of standard deviation of IA9; the correlation coefficient is ranging between 0.5 and 0.9 in those domains. Strong relationships between NP4 and IA9 are found in all areas with large interannual variability of IA9.

Summary and discussion

Winter ice motion and resulting redistribution of sea ice is one of the important factors determining summer ice extent. We conjecture that ice thickness distribution in spring is influenced by redistribution of ice floes during winter.

There are other factors controlling the spring ice thickness. One is the small-scale ice process. This study,

Citation: *Polar Research* 2013, *32*, 20193, http://dx.doi.org/10.3402/polar.v32i0.20193

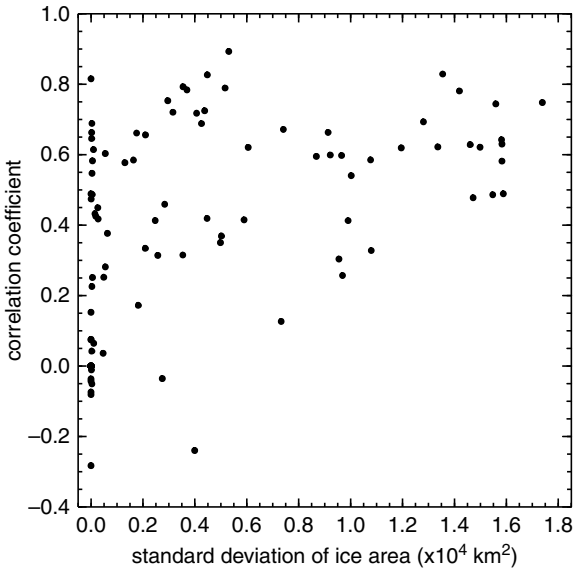

Fig. 7 Scatterplot of the derived correlation coefficient shown in Fig. 6a versus standard deviation of total ice area on 10 September (IA9) shown in Fig. 5a for the 108 domains.

based on 37.5-km resolution AMSR-E data, cannot directly detect the ice thickening through rafting/ridging of ice floes and new ice production in leads, which generally occurs at smaller scales. Though we can detect the possibility of them based on large-scale ice divergence/convergence, the ice deformation due to small-scale phenomena (ocean eddy, ice-floe interaction, etc.) should be considered in future. This study also ignored the thermodynamic ice thickening/thinning during December–April and spatial difference of ice thickness at the beginning of December. Therefore, we expect our method to be mainly valid for the seasonal ice cover, which now is the dominant ice type in the Arctic. Additionally, ice processes after May containing ice movement and melting are also attributed to the summer weather condition. For example, the correlation coefficient between NP4 and IA9 is 0.30 in a black domain in Fig. 6a in spite of relatively large interannual variability (1.0×10^4 km^2). The low correlation is strongly due to an event occurred in summer 2007; the unprecedented retreat of ice area around this domain was enhanced by a strong poleward wind field (Ogi et al. 2008), which is not considered in our analysis. The point is that even though these processes were not taken into consideration, the linear relation between the winter ice motion and summer ice cover is still significant in many regions with large interannual variability.

Steep regression lines in Fig. 6b–d are also seen in most of domains. It shows that the remaining ice area (IA9) is not directly related to a thick ice area in April (NP4). Some positive feedback processes, such as ice–ocean albedo feedback (Nihashi & Cavalieri 2006), play an important role in the fast retreat of ice. To reveal the processes behind this relation, we first need to clarify the process of ice retreat by dividing it into dynamic and thermodynamic effects employing a technique used by Kimura & Wakatsuchi (2011) and Holland & Kwok (2012).

Similar to the summer ice area, long-term trends are also seen in the winter ice velocity. Sea-ice drift speed has become faster in recent decades (Spreen et al. 2011). The winter redistribution of sea ice focused on in this study is strongly related to ice drift speed: the acceleration of the drift speed with the years brings larger outflow of the particles. Therefore, our method implicitly takes into account the long-term change in ice motion as well as year-to-year difference.

The pattern of winter ice redistribution is controlled by the atmospheric circulation because temporal changes in the winter ice motion are mainly controlled by the wind field (Kimura & Wakatsuchi 2000). In other words, Arctic sea ice acts as a "memory" of the winter atmospheric condition until the following summer.

Based on the linear relationship between NP4 and IA9, we can potentially improve the prediction of the summer ice area in spring by analysing the satellite-derived winter ice motion. This medium-term forecast looking several months ahead is useful for human activity in the Arctic, for example to determine whether or not the shipping route through the Arctic—the Northern Sea Route—will be navigable. Advanced Microwave Scanning Radiometer 2 (AMSR2), a successor of AMSR-E, which started observation in July 2012, should be a powerful tool for the future analyses. Additionally, data from a satellite-based altimeter, such as ICESat or CryoSat, will be also useful for this prediction.

Acknowledgements

The authors thank the National Snow and Ice Data Center for the gridded AMSR-E and IABP data. The figures were produced using the GFD Dennou Library software. This study was supported by the Green Network of Excellence Program Arctic Climate Change Research Project.

References

Cavalieri D.J., Markus T. & Comiso J.C. 2003. *AMSR-E/Aqua Daily L3 12.5 km brightness temperature, sea ice concentration, & snow depth polar grids*. Version 2. Boulder: National Snow and Ice Data Center.

Cavalieri D.J., Markus T. & Comiso J.C. 2004. *AMSR-E/Aqua Daily L3 6.25 km 89 GHz brightness temperature polar grids*. Version 2. Boulder: National Snow and Ice Data Center.

Colony R. & Rigor I. 2002. *IABP drifting buoy pressure, temperature, position, and interpolated ice velocity*. Boulder: National Snow and Ice Data Center.

Comiso J.C., Parkinson C.L., Gersten R. & Stock L. 2008. Accelerated decline in the Arctic sea ice cover. *Geophysical Research Letters 35*, L01703, doi: 10.1029/2007GL031972.

Emery W.J., Fowler C.W., Hawkins J. & Preller R.H. 1991. Fram Strait satellite image-derived ice motion. *Journal of Geophysical Research—Oceans 96*, 4751–4768.

Holland P.R. & Kwok R. 2012. Wind-driven trends in Antarctic sea-ice drift. *Nature Geoscience 5*, 872–875.

Kimura N. & Wakatsuchi M. 2000. Relationship between sea-ice motion and geostrophic wind in the Northern Hemisphere. *Geophysical Research Letters 27*, 3735–3738.

Kimura N. & Wakatsuchi M. 2004. Increase and decrease of sea ice area in the Sea of Okhotsk: ice production in coastal polynyas and dynamical thickening in convergence zones. *Journal of Geophysical Research—Oceans 109*, C09S03, doi: 10.1029/2003JC001901.

Kimura N. & Wakatsuchi M. 2011. Large-scale processes governing the seasonal variability of the Antarctic sea ice. *Tellus Series A 63*, 828–840.

Kwok R. 2006. Contrasts in sea ice deformation and production in the Arctic seasonal and perennial ice zones. *Journal of Geophysical Research—Oceans 111*, C11S22, doi: 10.1029/2005JC003246.

Kwok R., Cunningham G.F., Wensnahan M., Rigor I., Zwally H.J. & Yi D. 2009. Thinning and volume loss of the Arctic Ocean sea ice cover: 2003–2008. *Journal of Geophysical Research—Oceans 114*, C07005, doi: 10.1029/2009JC005312.

Markus T. & Cavalieri D.J. 2000. An enhancement of the NASA Team sea ice algorithm. *IEEE Transactions on Geoscience and Remote Sensing 38*, 1387–1398.

Melling H. & Riedel D.A. 1995. The underside topography of sea ice over the continental shelf of the Beaufort Sea in the winter of 1990. *Journal of Geophysical Research—Oceans 100*, 13641–13653.

Nihashi S. & Cavalieri D.J. 2006. Observational evidence of a hemispheric-wide ice–ocean albedo feedback effect on Antarctic sea-ice decay. *Journal of Geophysical Research—Oceans 111*, C12001, doi: 10.1029/2005JC003447.

Ninnis R.M., Emery W.J. & Collins M.J. 1986. Automated extraction of pack ice motion from advanced very high resolution radiometer imagery. *Journal of Geophysical Research—Oceans 91*, 10725–10734.

Ogi M., Rigor I.G., McPhee M.G. & Wallace J.M. 2008. Summer retreat of Arctic sea ice: role of summer winds. *Geophysical Research Letters 35*, L24701, doi: 10.1029/2008GL035672.

Ogi M., Yamazaki K. & Wallace J.M. 2010. Influence of winter and summer surface wind anomalies on summer Arctic sea ice extent. *Geophysical Research Letters 37*, L07701, doi: 10.1029/2009GL042356.

Perovich D.K., Light B., Eicken H., Jones K.F., Runciman K. & Nghiem S.V. 2007. Increasing solar heating of the Arctic Ocean and adjacent seas, 1979–2005: attribution and role in the ice albedo feedback. *Geophysical Research Letters 34*, L19505, doi: 10.1029/2007GL031480.

Rigor I.G., Wallace J.M. & Colony R.L. 2002. Response of sea ice to the Arctic Oscillation. *Journal of Climate 15*, 2648–2663.

Rothrock D.A., Percival D.B. & Wensnahan M. 2008. The decline in Arctic sea-ice thickness: separating the spatial, annual, and interannual variability in a quarter century of submarine data. *Journal of Geophysical Research—Oceans 113*, C05003, doi: 10.1029/2007JC004252.

Shimada K., Kamoshida T., Itoh M., Nishio S., Carmack E., McLaughlin F., Zimmermann S. & Proshutinsky A. 2006. Pacific Ocean inflow: influence on catastrophic reduction of sea ice cover in the Arctic Ocean. *Geophysical Research Letters 33*, L08605, doi: 10.1029/2005GL025624.

Spreen G., Kwok R. & Menemenlis D. 2011. Trends in Arctic sea ice drift and role of wind forcing: 1992–2009. *Geophysical Research Letters 38*, L19501, doi: 10.1029/2011GL048970.